Research Square

Preprints are preliminary reports that have not undergone peer review.
They should not be considered conclusive, used to inform clinical practice,
or referenced by the media as validated information.

A Polyphenolic Compound Amelirotates Mitochondrial Dysfunction in Human Cardiomyocyte Like Cells Subjected to Insulin-Resistant Senescence or β-Adrenergic Stress

Lubne Aljaser
Ankara University
Pinar Cevikbas Ilik
Lokman Hekim Üniversitesi
Yasemin Atici
Lokman Hekim Üniversitesi
Atakan Saglam
Ankara University
Deniz Billur
Ankara University
Yusuf Olgar
Ankara University
Belma TURAN
belma.turan@lokmanhekim.edu.tr
Lokman Hekim Üniversitesi

Research Article

Keywords: Heart function, metabolic syndrome, aging, mitochondria, natural nutrients, polyphenolic compounds

Posted Date: September 17th, 2026

DOI: https://doi.org/10.21203/rs.3.rs-10888122/v1

License: This work is licensed under a Creative Commons Attribution 4.0 International License.
Read Full License

Additional Declarations: No competing interests reported.

Abstract

Purpose: Metabolic and β-adrenergic stress are major contributors to cardiac dysfunction and may converge on mitochondrial dysfunction and oxidative stress. A Canadian pine bark extract (CPBE), a polyphenol-rich formulation, has been associated with beneficial cardioprotective effects. However, its direct effects on mitochondrial function in human cardiomyocytes exposed to distinct pathological stressors remain incompletely understood. We hypothesized that CPBE exerts cardioprotective effects by restoring mitochondrial redox homeostasis in AC16 cells subjected to aging combined with metabolic stress or a direct β-adrenergic stress.

Methods: Human AC16 cardiomyocyte-like cells were used to establish two distinct models of cardiac stress. Cells were treated with palmitic acid (PA) and D-galactose (D-gal) to mimic an insulin-resistant senescent heart (IRSH), or with isoproterenol (ISO) to model an ISO-induced hypertrophic heart (IIHH), followed by CPBE treatment. Mitochondrial function, cellular morphology, and redox status were comprehensively evaluated by assessing mitochondrial membrane potential (MMP), reactive oxygen species (ROS) production, antioxidant defense parameters, intracellular pH, ATP levels, and inflammatory and apoptotic markers using complementary electrophysiological, histological, and biochemical analyses. Results were compared with those obtained from untreated control cells.

Results: CPBE treatment significantly improved mitochondrial membrane potential and normalized mitochondrial fission markers in both the IRSH and IIHH models. It also reduced elevated ROS levels, restored intracellular ATP content, and attenuated inflammatory and apoptotic responses, parallel to improved cell morphology by reducing cell area, decreasing phagocytic vacuole accumulation, and restoring the cellular aspect ratio. Also, CPBE enhanced the balance between oxidative stress and the antioxidant defense system, and restored intracellular pH, indicating improved cellular metabolic and mitochondrial homeostasis.

Conclusions: These findings suggest that aging combined with either metabolic or β-adrenergic stress converges on a common pathway of mitochondrial redox dysfunction in human cardiomyocyte-like cells. CPBE appears to counteract these pathological alterations through multifaceted mitochondrial and redox-modulating mechanisms. Collectively, these results provide a mechanistic rationale for further investigation of CPBE as a potential mitochondria-targeted therapeutic strategy for cardiometabolic and stress-related cardiac dysfunction.

Highlights

* Metabolic and β-adrenergic stress converge on mitochondrial redox dysfunction.

* A polyphenolic Canadian pine bark–derived extract (CPBE) restores mitochondrial membrane potential and ATP production.

* CPBE reduces oxidative stress while enhancing antioxidant defense.

* CPBE improves mitochondrial dynamics and cellular morphology.

* CPBE represents a promising therapeutic candidate for cardiometabolic dysfunction.

Introduction

Heart failure, which often develops from chronic cardiac dysfunction, is a major cause of morbidity and mortality and represents one of the leading discharge diagnoses, particularly in older adults [1–4], while aging is strongly associated with heart failure [5, 6]. Cardiovascular aging is characterized by progressive structural, metabolic, and electrophysiological remodeling, ultimately predisposing the heart to dysfunction and failure [7–9]. Among the underlying mechanisms, mitochondrial dysfunction and excessive production of reactive oxygen species (ROS) have emerged as central drivers of age-related cardiac deterioration [10, 11]. While physiological levels of ROS are essential for intracellular signaling, their uncontrolled accumulation disrupts redox homeostasis, impairs mitochondrial bioenergetics, and contributes to contractile dysfunction, arrhythmogenesis, and endothelial impairment [12–17]. Aging is frequently accompanied by metabolic disturbances, including insulin resistance, which further exacerbates cardiac vulnerability [15, 18, 19]. Impaired insulin signaling alters substrate utilization, disrupts mitochondrial dynamics, and enhances oxidative stress, thereby promoting adverse cardiac remodeling. Experimental and clinical evidence indicates that insulin resistance not only contributes to metabolic inflexibility but also modulates sympathetic activity and accelerates the progression toward heart failure. Consistent with this, previous studies have demonstrated significantly elevated systemic oxidative stress and increased ROS production in cardiomyocytes isolated from aged and insulin-resistant models, highlighting mitochondria as a critical therapeutic target. Given the pivotal role of mitochondrial dysfunction in cardiac aging and disease, strategies aimed at restoring redox balance and improving mitochondrial function have gained considerable attention.

Nutritional supplementation has emerged as a promising adjunct approach, particularly under conditions of inadequate dietary intake or increased metabolic demand [20]. Certain bioactive compounds can act as mitochondrial-targeted antioxidants, supporting ATP production, modulating immune responses, and improving overall metabolic homeostasis. Among these, pine bark-derived extracts have attracted significant interest due to their high content of polyphenols, including procyanidins, catechins, and phenolic acids. These compounds exhibit potent antioxidant and anti-inflammatory properties and have been associated with a range of cardiometabolic benefits, including improved endothelial function, reduced lipid accumulation, enhanced glucose regulation, and attenuation of inflammatory pathways [21–25]. Among their reported benefits, there are reductions in lipid accumulation and oxidative stress in biological samples [26–29]. Pine bark extracts have also been reported to exert cytoprotective effects in vascular and metabolic disorders such as hyperlipidemia, atherosclerosis, and diabetes [30–33].

Commercial formulations of pine bark extract, most commonly derived from maritime pine species, are often enriched with additional bioactive components such as rose hips and vitamin C, which may further enhance antioxidant capacity and biological efficacy. Despite accumulating evidence supporting their

systemic benefits, the direct effects of such formulations on cardiac mitochondrial structure and function, particularly in the context of aging, insulin resistance, and heart failure, remain insufficiently understood [34–38]. Importantly, previous work from our group demonstrated that pharmacological targeting of mitochondrial ROS using MitoTEMPO leads to marked improvements in mitochondrial membrane potential and overall cardiomyocyte function in aged models. These findings underscore the therapeutic relevance of mitochondrial redox modulation and suggest that nutraceutical compounds with similar antioxidant properties may offer comparable benefits [10, 11].

Therefore, the present study aimed to investigate the effects of a Canadian pine bark extract (CPBE), enriched with rose hips and vitamin C, on mitochondrial structure and function in PA and D-gal treated AC16 cells to mimic insulin-resistant senescence heart (IRSH) as well as isoproterenol-treated AC16 cells to mimic ISO-induced hypertrophic heart (IIHH) under in vitro conditions. Using a combination of electrophysiological, histological, and biochemical approaches, we sought to determine whether CPBE supplementation can attenuate mitochondrial dysfunction and improve cellular integrity in these clinically relevant models.

Materials & Methods

Culturing AC16 Human Cardiomyocyte Cell Line

AC16 cells, a commonly used human cardiomyocyte line, are maintained under defined culture conditions to preserve their growth ability and cardiomyocyte-like features. The cells are routinely cultured in Dulbecco's Modified Eagle Medium (DMEM) containing 10% fetal bovine serum (FBS), 1% penicillin-streptomycin, and L-glutamine, and kept at 37°C in a humidified incubator with 5% CO_2. The culture medium is replaced every 2–3 days to maintain optimal conditions. When the cells reach roughly 80% confluence, they are passed using 0.05% trypsin-EDTA [39].

IRSH cellular model for the first time was established in our laboratory. Briefly, cells were co-incubated with 50 μM PA and 50 mg/mL D-gal for 24 hours to establish an insulin-resistant senescent cell model, which PA inducing insulin resistance and D-gal promoting cellular senescence [4, 40, 41]. The successful establishment of the model was confirmed by a glucose uptake assay and a β-galactosidase senescence kit, together with elevated ROS levels, increased phosphorylated H2AX at Ser139 and impaired mitochondrial function [41]. AC16 cardiomyocytes were also treated with 10 μM isoproterenol (ISO) for 24 h to establish IIHH, an in vitro hypertrophic heart model. The concentration was selected based on preliminary optimization experiments and previous studies using ISO-induced hypertrophy models [42, 43]. Following model establishment, the cells were treated with the extract (50 μg/mL) for same incubation period to evaluate its potential protective effects. The experimental procedures to mimic pathological cardiomyocytes in AC16 cells are presented in Fig. 1.

Determination of Reactive Oxygen Species Production Level

ROS levels in AC16 cardiomyocyte-like cells were measured using the fluorescent probe 2',7'-dichlorodihydrofluorescein diacetate (DCFH-DA). This non-fluorescent dye enters cells and is converted by intracellular esterases to DCFH, which is then oxidized by ROS to the fluorescent product DCF. AC16 cells were incubated with 10 μM dye solution for 45 minutes at 37°C in the dark. After staining, cells were washed three times with PBS to remove excess dye. Fluorescence was detected using a Leica TCS SP5 confocal fluorescence microscope, with excitation at 485 nm and emission at 530 nm. Images were captured at 1024×1024 resolution, and ROS intensity was quantified using LAS X software (Leica Microsystems). For assay validation and quantification (higher florescence intensity represents lower ROS level at resting) cells were treated with 100 μM H_2O_2, producing a clear fluorescence increase and confirming assay sensitivity [44].

Mitochondrial Membrane Potential Measurements

Mitochondrial membrane potential in AC16 human cardiomyocytes was assessed using potentiometric fluorescent probe JC-1. Cells were incubated with 5 μM JC-1 for 30 minutes at 37°C and then imaged using a Leica TCS SP5 confocal fluorescence microscope. Green fluorescence from JC-1 monomers was detected using a 488 nm filter, while red fluorescence from JC-1 aggregates was captured using a 559 nm filter. Carbonyl cyanide 4-(trifluoromethoxy) phenylhydrazone (FCCP; 5 μM) served as a positive control for mitochondrial depolarization. Green-to-red fluorescence analysis was performed using LAS X software, as previously described [14].

Cytosolic pH Measurements

Intracellular pH in AC16 human cardiomyocyte-like cells was assessed using the pH-sensitive fluorescent probe SNARF-1 AM. Cells were loaded with 5 μM SNARF-1 AM for 30 minutes at 37°C, and imaging was performed with a Leica TCS SP5 confocal microscope. Excitation was set at 543 nm, and emission signals were collected at 580 nm and 640 nm. Cytosolic pH variations were quantified by the fluorescence intensity ratio of 580 nm to 650 nm (described as relative acidosis), allowing accurate evaluation of intracellular pH changes [45, 46].

All fluorescence images were analyzed using region-of-interest (ROI)-based image analysis. ROIs were manually delineated around individual cells, and the mean fluorescence intensity within each ROI was quantified. For ratiometric fluorescence probes, fluorescence intensity ratios were calculated from the corresponding emission channels and used for subsequent analyses.

Histological analysis

Electron microscopy (EM) analysis was performed on cultured human cardiomyocytes, as previously described [43]. The cells were fixed in phosphate buffer (pH 7.3) containing 2.5% glutaraldehyde and 2% paraformaldehyde, followed by washing with phosphate-buffered saline (PBS, pH 7.3). The samples were then post-fixed in 0.1 M phosphate buffer containing 1% osmium tetroxide for 2 hours. After dehydration through a graded ethanol series, the specimens were embedded in Araldite 6005 and sectioned using a

Leica Ultracut R ultramicrotome (Leica, Solms, Germany). Ultra-thin sections were stained with uranyl acetate and lead citrate and examined using an HT 7800 TEM (Hitachi High-tech, Tokyo, Japan). As described previously [44, 45], all images were digitized and quantified using the EMIP software on the HT 7800 TEM (Hitachi High-tech, Tokyo, Japan).

Biochemical analysis: Levels of SIRT1, SIRT3, cyclic guanosine monophosphate (cGMP), BNIP3, ATP, ADP, cyclic adenosine monophosphate (cAMP), Dynamin-1-like protein (DMN1L/DRP1), NLR family pyrin domain-containing protein 3 (NLRP3), B-cell lymphoma/leukemia 2 (Bcl-2), Bcl-2-associated X protein (BAX), 4-hydroxynonenal (4-HNE), nuclear factor kappa B p65 subunit (NF-κB p65), and nuclear factor erythroid 2-associated factor 2 (NRF-2) were measured using commercially available enzyme-linked immunosorbent assay (ELISA) kits. The kits used in the study were as follows: SIRT1 (Elabscience, Cat. No: E-EL-R1102), SIRT3 (BT Lab, Cat. No: E1304Ra), cGMP (BT Lab, Cat. No: E0297Ra), BNIP3 (BT Lab, Cat. No: E0826Ra), ATP (BT Lab, Cat. No: E0920Ra), ADP (BT Lab, Cat. No: EA0172Ra), cAMP (Elabscience, Cat. No: E-EL-0056), DMN1L (BT Lab, Cat. No: E3356Ra), NLRP3 (BT Lab, Cat. No: E1627Ra), Bcl-2 (Elabscience, Cat. No: E-EL-R0096), BAX (Elabscience, Cat. No: E-EL-R0098), 4-HNE (Elabscience, Cat. No: E-EL-R0098). E-EL-0128), NF-κB p65 (Elabscience, Cat. No: E-EL-R0674) and NRF-2 (BT Lab, Cat. No: E2184Ra). The analytical performance characteristics of the kits are within the ranges specified by the manufacturers. Sensitivity and measurement ranges are as follows: SIRT1 (0.1 ng/mL; 0.16–10 ng/mL), SIRT3 (0.04 ng/mL; 0.1–40 ng/mL), cGMP (0.52 pmol/mL; 1–300 pmol/mL), BNIP3 (2.51 ng/L; 5–1000 ng/L), ATP (2.57 ng/mL; 5–1500 ng/mL), ADP (0.07 µg/mL; 0.16–10 µg/mL), cAMP (0.94 ng/mL; 1.56–100 ng/mL), DMN1L (72.5 ng/L; 156.25–10000 ng/L), NLRP3 (0.021 ng/mL; The values were determined as follows: Bcl-2 (0.05–20 ng/mL), Bax (0.1 ng/mL; 0.16–10 ng/mL), 4-HNE (0.38 ng/mL; 0.63–40 ng/mL), NF-κB p65 (46.88 pg/mL; 78.13–5000 pg/mL) and NRF-2 (9.64 ng/L; 20–4500 ng/L). The intra-assay and inter-assay coefficients of variation (CV) for all parameters were < 10% and < 8%, respectively, which are within acceptable limits. Measurements were performed in accordance with the manufacturer's instructions.

Statistical analysis

All statistical analyses were performed using the SPSS software (version 27.0). The normality of the data distribution was assessed using the Shapiro–Wilk test. Variables with a normal distribution were analyzed using one-way analysis of variance (one-way ANOVA), followed by Tukey's multiple comparisons test. Variables that did not meet the assumption of normality were analyzed using the Kruskal–Wallis test, followed by Bonferroni-adjusted multiple comparisons. Data are presented as mean ± standard error of the mean (SEM), and a p value < 0.05 was considered statistically significant.

Results

The CPBE application restored mitochondrial membrane potentials in both insulin-resistant senescent and heart

failure-modeled cells

To evaluate the beneficial effects of CPBE on cardiac health independent of systemic factors, we assessed MMP in IRSH and IIHH AC16 cell models treated with 50 μg/mL of CPBE for 24 h. MMP was determined via JC-1-loaded fluorescent imaging, where an increased fluorescence intensity ratio ($F_{535/585}$) indicated MMP depolarization due to elevated dye-monomer formation. Our results demonstrated that both the IRSH and IIHH groups exhibited significantly higher JC-1 intensity compared to their respective Con groups. Notably, while the IRSH model displayed more severe depolarization, CPBE treatment resulted in a statistically significant recovery of MMP in both the IRSH and IIHH models (Fig. 2).

CPBE treatment reversed mitochondrial morphological changes in cells from both the IRSH and IIHH groups

To confirm the depolarization in the MMPs, whether associated with the structural changes in the mitochondria, we first examined mitochondrial function and fine ultrastructure in these modeled cells. The representative transmission electron microscopy (TEM) micrographs are giving in Fig. 3 (A and B) for experimental groups. The ultrastructure of cells from the Con group basically displayed typical normal cardiomyocytes features, including an elliptical shape, well-organized cristae, and an electron-lucent matrix in both (A, upper part) and (B, upper part). As indicated by various symbols, the alterations in the experimental group of cells, there are degenerative mitochondria exhibiting smaller mitochondiom with elliptical or rounded morphology, as well as prominent cristae loss and disorganization, numerous autophagic vacuoles, and some containing undigested mitochondrial debris. The CPBE treatment of the experimental groups of cells provided not a complete recovery in mitochondrial ultrastructure, characterized with a limited number of mitochondria with preserved normal morphology and appearance of slightly degenerated mitochondria, and a reduced number of autophagic vacuoles in the cells from IRSH and IIHH groups, indicating partial restoration of mitochondrial ultrastructure with CPBE application.

We also quantified the alterations in TEM data and calculated the cell area, aspect ratio (length to width ratio) and phagocytic vacuole per cell. As can be seen in Fig. 3 (lower parts in A and B), the mean value (± SEM) values calculated for both IRSH and IIHH groups were significantly increased compared to those of controls, while these values were found to be normalized in the CPBE group (lower parts, left side). The aspect ratios in both IRSH and IIHH groups were signigicantly decreased compared to the controls with significant recoveris with the CPBE treatment (lower parts, middile part). The decreased level in aspect ration can point out the existence of high level fission in the cells. The last parameters calculated from the TEM data were phagocytic vacuoles determined per cell (lower parts, right side). These mean values were 3-fold higher in these two groups while there were normalization with the CPBE treatment. These values also represent an increased phagocytic activity, damage in cells, and increased autophagy in both IRSH and IIHH groups.

Treatment of the IRSH group with CPBE provided significant recoveries in cellular acidosis status and the ROS status of the cells

We further examined the relative acidosis status in the cells from both the IRSH and IIHH groups (Fig. 4). The experimental protocol to determine the ROS levels is given in Fig. 4A. The representative cells during experimental period are given in the left panel in B and upper panel in C. The Snarf-loaded intensity experiments showed that neither IRSH nor IIHH exhibited a significant effect on intracellular acidosis. However, CPBE treatment was associated with a modest increase in intracellular pH, suggesting a potential influence on intracellular pH homeostasis. Since neither pathological model altered intracellular acidification, this finding should be considered supportive rather than indicative of a reversal of disease-associated acidosis.

In another set of experiments, we monitored ROS levels in the modeled cardiomyocytes and then their responses by challenging them with H_2O_2 where higher fluorescence intensity indicates lower ROS levels at resting conditions. The representative original cell images are given in the left part of Fig. 5 (A and B). The DCF fluorescence intensity in response to 100 μM H_2O_2 in the IRSH group was significantly lower than that of the Con group (Fig. 5A). Similarly, the H_2O_2-evoked fluorescence intensity was also significantly lower than that of the Con group in IIHH cells (Fig. 5B), as well. The CPBE treatment markedly increased the H_2O_2-induced fluorescence intensity in both modeled groups, with a greater effect observed in the IIHH group, suggesting its more pronounced substantial role (even over the Con group) in modulating oxidative stress in the cells from the IIHH group than that of cells from the IRSH group.

Modulation of Oxidative Stress, Inflammatory, and Apoptotic Markers by CPBE in IRSH and IIHH Cells

To confirm the functional and ultrastructural data associated with CPBE application on mitochondria, we performed some biochemical analysis. We first examined the oxidative stress status by determination of 4-HNE level, which is a damage marker known as toxic lipid oxidation product and can induce mitochondrial dysfunction and increase apoptosis and inflammation at high levels. The 4-HNE levels in both the IRSH group and IIHH group were found to be significantly higher than that of the Con group while these increses were reversed by CPBE application (Fig. 6A). For further validation, we determined the levels of NRF-2, a transcription factor of antioxidative defense of cells. As can be seen in Fig. 6B, the NRF-2 levels were significantly depressed in both experimental groups of cells comparison to the Con group, whereas, CPBE application could normalize these levels fully in both experimental groups.

In the second part of this group biochemical analysis, we primarily performed evaluations to assess the activation status of the inflammatory response in cells from the experimental groups. We examined the status of NF-κB and NLRP3 in these cells. First, we examined the levels of NF-κB in these cells, which is an important transcriptional factor to start inflammation. As can be seen in Fig. 6C, the CPBE application

could normalize the over-increased NF-κB levels in these experimental groups of cells. Another factor in this group of analysis was to determine the levels of NLRP3, which is the main sensor of an inflammasome complex within the cell and activates inflammation. The NLRP3 levels were found not to be different in the experimental groups compared to the Con group while there was no significant effect with CPBE (Fig. 6D).

We also analyzed BNIP3 status of the cells, which is a pro-apoptotic and mitophagy-related protein and plays a key role in mitochondrial quality control under stress conditions, especially high ROS production. There was a slight but significant increase in BNIP3 level in the IRSH group with a further slight but significant increase under CPBE application (Fig. 6E, left), this increase in the IIHH group was significantly recovered with the CPBE application (Fig. 6E, right).

Since BCL-2 and BAX are two critical proteins that regulate the mitochondrial pathway of apoptosis and should be interpreted together, in the last part of this group of evaluations, we also examined the levels of BCL-2 and BAX. Although the BCL-2 levels were not significantly different among all groups, the BAX levels significantly increased in both experimental groups, and the CPBE application could normalize these levels in both groups (Fig. 6F and G, respectively). The ratios of BAX to BCL-2 for the groups are shown in Fig. 6H. These ratios in both experimental groups are significantly higher than those of the Con group; the CPBE application could induce significant recoveries in these parameters.

Effects of CPBE application on mitochondrial metabolism

Since some cross-pathways are important through their collective regulation of mitochondrial integrity, energy production, and survival signaling, and determine whether a stressed cell adapts or undergoes death, we determined some parameters stasus such as SIRT1, SIRT3, DRP1, cAMP, cGMP, ATP, and ADP levels in all groups of cells from both the IRSH and IIHH groups (Fig. 7, A to G). The levels of SIRT1 and SIRT3 (mostly associated with intracellular ROS and ATP levels in the cells) in the IRSH group were slightly but significantly decreased, while there were full normalizations in these parameters by CPBE treatment (Fig. 7, left panels of A and B). The decreases in the levels of both SIRT1 and SIRT3 are more pronounced in the IIHH groups compared to the IRSH group, while there were again full recoveries in these parameters with CPBE application.

To determine the mitochondrial fission dynamics, we determined the levels of DRP1. As can be seen in Fig. 7C, the levels of DRP1 were significantly increased in both experimental groups of cells compared to those of controls, with higher levels in the IIHH group than in the IRSH group, and the CPBE application could normalize these depressions to the level of the Con group, fully. For further analysis, we determined the levels of cGMP and cAMP. The cGMP levels were significantly high in these experimental groups compared to the controls. The CPBE application could be fully normalized in these experimental cells (Fig. 7, D and E, respectively).

Since the energy status of the cells can be determined by measuring the ATP to ADP ratio in cells, we determined both the levels of ATP and ADP and then calculated their ratio (Fig. 7F and G, respectively). Although the ADP levels were similar among all groups, the ATP levels were found to be depressed significantly in both experimental groups compared to those of the Con group, while the CPBE application could significantly reverse the level of the Con group. The ratios of ATP to ADP of both groups are given in Fig. 7H. This ratio was significantly lower in both experimental groups than in the Con group. The CPBE application could recover these decreases, significantly.

Discussion

Nutritional supplements may support human health and cardiac function, especially under conditions of insufficient dietary intake, by addressing nutritional deficiencies and enhancing energy metabolism, immune responses, and overall metabolic health. Certain dietary supplements have been reported to act as mitochondrial antioxidants and to support energy production in cardiac myocytes, potentially reducing oxidative stress and contributing to the regulation of cardiac rhythm, muscle contraction, and endothelial function. Among natural nutritional supplements, pine-derived products are rich in polyphenols and proanthocyanidins, providing beneficial cardiovascular effects [20]. Pine bark extract contains high levels of polyphenols with antioxidant and cytoprotective properties against oxidative damage in human endothelial cells and has been reported to improve hyperlipidemia, atherosclerosis, diabetes, and inflammatory conditions[32, 50–52]. Such extracts are rich in polyphenols, especially procyanidins, catechins, and phenolic acids, which exhibit strong antioxidants and anti-inflammatory activity. Additionally, studies have reported cardioprotective, vasoprotective, neuroprotective, and antidiabetic effects through improved glucose regulation and insulin sensitivity [23, 53–58].

In the present study, we demonstrate that CPBE treatment restores mitochondrial dysfunction and cellular homeostasis in human cardiac cells modeled to IRSH and IIHH conditions. Using AC16 cells as an in vitro model of metabolic and structural cardiac stress [11, 17, 47], we observed significant depolarization of MMP and increases in ROS production in both IRSH and IIHH groups. The CPBE treatment effectively normalized these mitochondrial parameters, indicating a direct cardioprotective effect independent of systemic factors.

The histological analysis demonstrated that the increased cardiomyocyte cell area observed in our modelled cells reflects the induction of pathological hypertrophic remodeling. In contrast, the marked reduction in cell area following CPBE treatment indicates that the compound attenuates the hypertrophic response and promotes the restoration of normal cardiomyocyte morphology. These morphological improvements are likely associated with the ability of CPBE to reduce ROS production and oxidative stress while preserving mitochondrial function. Importantly, these interpretations are strongly supported by our functional and biochemical findings.

Furthermore, the significant reduction in the number of cytosolic phagocytic vacuoles following CPBE treatment provides additional evidence for its protective effects against cellular degeneration. This

observation suggests preservation of cardiomyocyte ultrastructure and attenuation of pathological remodeling. Overall, the decrease in phagocytic vacuoles indicates reduced ultrastructural damage and restoration of cellular homeostasis. These findings are consistent with diminished oxidative stress, improved mitochondrial quality control, and reduced degradation of damaged intracellular components, further supporting the cardioprotective properties of CPBE.

In addition, the recovery of the cardiomyocyte aspect ratio following CPBE treatment further reinforces its beneficial effects on cellular architecture. Restoration of the aspect ratio toward control values is commonly interpreted as preservation or recovery of the normal elongated cardiomyocyte phenotype and attenuation of pathological structural remodeling. Together, the improvements in cell area, phagocytic vacuole accumulation, and aspect ratio demonstrate that CPBE effectively mitigates cardiomyocyte hypertrophy and structural degeneration while preserving cellular integrity, findings that are in agreement with the accompanying biochemical and functional data.

CPBE application protect mitochondrial function via regulation of oxidative stress in both IRSH and IIHH

Mitochondrial dysfunction is a hallmark of aging and heart failure, often associated with ROS overproduction and lipid peroxidation [59]. Our data demonstrate that 4-HNE levels, a toxic lipid peroxidation product, were significantly elevated in cells from both IRSH and IIHH groups, consistent with increased oxidative stress. CPBE effectively reduced 4-HNE accumulation, suggesting a mitigation of oxidative damage. Correspondingly, the transcription factor NRF2, a master regulator of cellular antioxidant defenses, was downregulated in stressed cells but restored by CPBE. These findings indicate that CPBE enhances endogenous antioxidant responses, likely contributing to improved mitochondrial integrity. Similar protective effects via NRF2 activation have been reported in cardiomyocytes exposed to oxidative stress [60].

CPBE application controls inflammation and inflammasome signaling in both IRSH and IIHH

We examined key inflammatory mediators, NF-κB and NLRP3, to assess the inflammasome and stress-induced inflammatory signaling. NF-κB, which primes inflammatory gene expression, was elevated in IRSH and IIHH cells and normalized following CPBE treatment. Interestingly, NLRP3 levels remained unchanged, suggesting that in this in vitro model, inflammasome assembly may require additional in vivo signals, or that CPBE specifically targets NF-κB-mediated priming rather than NLRP3 activation. These results are consistent with previous studies indicating that oxidative stress-induced NF-κB activation is a critical upstream event in cardiac inflammation [61].

CPBE application affects apoptosis and mitochondrial quality control in both IRSH and IIHH

Mitochondrial apoptosis is tightly regulated by the BCL-2 family proteins. In our models, Bax levels were significantly elevated while BCL-2 remained unchanged, reflecting a pro-apoptotic shift. CPBE effectively normalized BAX expression, indicating anti-apoptotic effects. BNIP3, a regulator of mitophagy and stress-induced apoptosis, was unchanged across groups, suggesting that CPBE's protective effects may be more directly related to mitochondrial stabilization and apoptosis inhibition rather than modulation of mitophagy pathways. These findings align with prior studies showing that targeted interventions can prevent oxidative stress-induced apoptosis in cardiomyocytes without necessarily altering basal BNIP3-mediated mitophagy [62].

CPBE application and bioenergetics, mitochondrial dynamics, and signaling in both IRSH and IIHH

Cellular energy balance and mitochondrial dynamics were significantly perturbed in IRSH and IIHH cells. Both SIRT1 and SIRT3, critical regulators of mitochondrial function and ROS detoxification, were downregulated, consistent with impaired metabolic adaptation under stress. DRP1, a key mediator of mitochondrial fission, was elevated, indicating increased mitochondrial fragmentation, a phenomenon linked to impaired ATP production and increased oxidative stress [63]. Accordingly, the ATP/ADP ratio was decreased, while cyclic nucleotide signaling was disrupted, with decreased cAMP and elevated cGMP. CPBE restored SIRT1/SIRT3 levels, normalized DRP1, improved ATP/ADP ratio, and balanced cyclic nucleotide signaling, demonstrating coordinated improvements in mitochondrial bioenergetics and cellular signaling. These results highlight the potential of CPBE to modulate energy metabolism, mitochondrial quality control, and adaptive signaling networks in stressed cardiac cells.

Integrative Mechanism by CPBE

Overall, our findings suggest that CPBE exerts multifaceted cardioprotective effects in insulin-resistant and heart failure-modeled human cardiomyocytes. By reducing oxidative stress, attenuating NF-κB-driven inflammation, modulating apoptosis, and restoring mitochondrial bioenergetics and signaling, CPBE promotes cellular resilience against metabolic and structural stressors. This integrated response is particularly important in aging and failing hearts, where mitochondrial dysfunction and oxidative stress form a self-reinforcing cycle that exacerbates cell death and functional decline [11, 59].

Study limitations

Although AC16 cells provide a well-established and reproducible human cardiomyocyte-like in vitro model for investigating cellular stress responses and mitochondrial biology, they are immortalized, proliferative, and non-contractile. Therefore, they do not fully reproduce the electrophysiological, metabolic, and contractile properties of adult human cardiomyocytes or the complexity of cardiac aging and heart failure. Another limitation of the present study is that intracellular protein levels were quantified using commercially validated ELISA kits without confirmation by complementary techniques such as Western blotting, immunofluorescence, or quantitative PCR. Although ELISA provides quantitative information on protein abundance, additional validation using orthogonal methodologies would further strengthen the mechanistic interpretation of the findings. Future studies incorporating

these complementary approaches will be valuable for confirming the observed molecular alterations. Consequently, the findings of the present study should be interpreted within the context of this experimental model. Future studies using primary adult cardiomyocytes and appropriate in vivo models will be necessary to validate the translational relevance of these findings.

Declarations

Competing interests

The authors declare no competing interests.

Use of Artificial Intelligence (AI)-Assisted Technology for manuscript preparation

The authors confirm that there was no use of AI-assisted technology for assisting in the writing of the manuscript and no images were manipulated using AI.

Funding

This study was supported by Lokman Hekim University Scientific Research Projects Coordination Unit. Project No.: TSA-2025-131.

Author Contribution

L. A., P. C. I., and Y. A. designed experiments and conducted most of the experiments. A. S. and D. B. performed histological analysis. Y. O. and B. T. are responsible for the data analysis and graphic design aspects and wrote the article.

Data availability

No datasets were generated or analysed during the current study.

Data Availability

The authors can confirm that all relevant data are included in the article which are open and transporant.

References

1. Montalto, M., et al., *Heart failure in older patients: an update.* Journal of clinical medicine, 2025. **14**(6): p. 1982.

2. Martínez-Braña, L., et al., *Clinical characteristics and prognosis of heart failure in elderly patients.* Revista Portuguesa de Cardiologia (English Edition), 2015. **34**(7–8): p. 457–463.

3. de Freitas, E.V., M. Batlouni, and R. Gamarsky, *Heart failure in the elderly.* Journal of geriatric cardiology: JGC, 2012. **9**(2): p. 101.

4. Debacq-Chainiaux, F., et al., *Protocols to detect senescence-associated beta-galactosidase (SA-βgal) activity, a biomarker of senescent cells in culture and in vivo.* Nature protocols, 2009. **4**(12): p. 1798–1806.

5. Lakatta, E.G. and D. Levy, *Arterial and cardiac aging: major shareholders in cardiovascular disease enterprises: Part II: the aging heart in health: links to heart disease.* Circulation, 2003. **107**(2): p. 346–354.

6. Tsao, C.W., et al., *Heart disease and stroke statistics—2022 update: a report from the American Heart Association.* Circulation, 2022. **145**(8): p. e153–e639.

7. Ferrucci, L. and E. Fabbri, *Inflammageing: chronic inflammation in ageing, cardiovascular disease, and frailty.* Nature Reviews Cardiology, 2018. **15**(9): p. 505–522.

8. Terman, A. and U.T. Brunk, *Lipofuscin.* The international journal of biochemistry & cell biology, 2004. **36**(8): p. 1400–1404.

9. Strait, J.B. and E.G. Lakatta, *Aging-associated cardiovascular changes and their relationship to heart failure.* Heart failure clinics, 2012. **8**(1): p. 143.

10. Olgar, Y., et al., *Aging related functional and structural changes in the heart and aorta: MitoTEMPO improves aged-cardiovascular performance.* Experimental Gerontology, 2018. **110**: p. 172–181.

11. Olgar, Y., et al., *MitoTEMPO provides an antiarrhythmic effect in aged-rats through attenuation of mitochondrial reactive oxygen species.* Experimental gerontology, 2020. **136**: p. 110961.

12. Evans, J.L. and I.D. Goldfine, *Aging and insulin resistance: just say iNOS.* Diabetes, 2013. **62**(2): p. 346.

13. Makrecka-Kuka, M., et al., *Empagliflozin protects cardiac mitochondrial fatty acid metabolism in a mouse model of diet-induced lipid overload.* Cardiovascular Drugs and Therapy, 2020. **34**(6): p. 791–797.

14. Tuncay, E., et al., *ZnT6-mediated Zn2 + redistribution: Impact on mitochondrial fission and autophagy in H9c2 cells.* Molecular and Cellular Biochemistry, 2025. **480**(7): p. 4283–4296.

15. Durak, A. and B. Turan, *Liraglutide provides cardioprotection through the recovery of mitochondrial dysfunction and oxidative stress in aging hearts.* Journal of physiology and biochemistry, 2023. **79**(2): p. 297–311.

16. Olgar, Y., et al., *Aging related functional and structural changes in the heart and aorta: MitoTEMPO improves aged-cardiovascular performance.* Exp Gerontol, 2018. **110**: p. 172–181.

17. Olgar, Y., et al., *Insulin acts as an atypical KCNQ1/KCNE1-current activator and reverses long QT in insulin-resistant aged rats by accelerating the ventricular action potential repolarization through affecting the β3-adrenergic receptor signaling pathway.* Journal of Cellular Physiology, 2022. **237**(2): p. 1353–1371.

18. Olgar, Y., A. Durak, and B. Turan, *Acute GLP-1 agonism induces arrhythmogenic electrical activity in aged mice heart through impaired cellular Na + and Ca2 + handlings: The role of CK2 hyperphosphorylation.* Anatolian Journal of Cardiology, 2025. **29**(2): p. 83.

19. Olgar, Y., et al., *Ticagrelor reverses the mitochondrial dysfunction through preventing accumulated autophagosomes-dependent apoptosis and ER stress in insulin-resistant H9c2 myocytes.* Molecular and Cellular Biochemistry, 2020. **469**(1): p. 97–107.

20. Dziedziński, M., J. Kobus-Cisowska, and B. Stachowiak, *Pinus species as prospective reserves of bioactive compounds with potential use in functional food—Current state of knowledge.* Plants, 2021. **10**(7): p. 1306.

21. Mohammadi, S., et al., *Does supplementation with pine bark extract improve cardiometabolic risk factors? A systematic review and meta-analysis.* BMC Complementary Medicine and Therapies, 2025. **25**(1): p. 71.

22. Hadi, A., et al., *Effects of strawberry supplementation on cardiovascular risk factors: a comprehensive systematic review and meta-analysis of randomized controlled trials.* Food & function, 2019. **10**(11): p. 6987–6998.

23. Yang, X. and K. Qian, *Protein O-GlcNAcylation: emerging mechanisms and functions.* Nat Rev Mol Cell Biol, 2017. **18**(7): p. 452–465.

24. Liu, R. and C.G. Proud, *Eukaryotic elongation factor 2 kinase as a drug target in cancer, and in cardiovascular and neurodegenerative diseases.* Acta Pharmacologica Sinica, 2016. **37**(3): p. 285–294.

25. Ohkita, M., Y. Kiso, and Y. Matsumura, *Pharmacology in health foods: improvement of vascular endothelial function by French maritime pine bark extract (Flavangenol).* Journal of pharmacological sciences, 2011. **115**(4): p. 461–465.

26. Nakayama, S., et al., *Pine bark extract prevents low-density lipoprotein oxidation and regulates monocytic expression of antioxidant enzymes.* Nutrition research, 2015. **35**(1): p. 56–64.

27. Shimada, T., et al., *Preventive effect of boiogito on metabolic disorders in the TSOD mouse, a model of spontaneous obese type II diabetes mellitus.* Evidence-Based Complementary and Alternative Medicine, 2011. **2011**(1): p. 931073.

28. Sugaya, M., et al., *Guidelines for the management of cutaneous lymphomas (2011): A consensus statement by the J apanese S kin C ancer S ociety–L ymphoma S tudy G roup.* The Journal of Dermatology, 2013. **40**(1): p. 2–14.

29. McGrath, K.C., et al., *Inhibitory Effect of a French Maritime Pine Bark Extract-Based Nutritional Supplement on TNF-α-Induced Inflammation and Oxidative Stress in Human Coronary Artery Endothelial Cells.* Evidence-Based Complementary and Alternative Medicine, 2015. **2015**(1): p. 260530.

30. Safaeian, L., et al., *Cardioprotective effects of Pinus eldarica bark extract on adrenaline-induced myocardial infarction in rats.* Asian Pacific Journal of Tropical Biomedicine, 2023. **13**(4): p. 148–155.

31. Hajhashemi, V., B. Zolfaghari, and P. Amin, *Anti-nociceptive and anti-inflammatory effects of hydroalcoholic extract and essential oil of Pinus eldarica in animal models.* Avicenna journal of phytomedicine, 2021. **11**(5): p. 494.

32. Huseini, H.F., et al., *Anti-hyperlipidemic and anti-atherosclerotic effects of Pinus eldarica Medw. nut in hypercholesterolemic rabbits.* DARU Journal of Pharmaceutical Sciences, 2015. **23**(1): p. 32.

33. Safaeian, L., et al., *Antioxidant and anti-hyperlipidemic effects of bark extract of Pinus eldarica in dexamethasone-induced dyslipidemic rats.* 2019.

34. YANG, H.M., et al., *A randomised, double-blind, placebo-controlled trial on the effect of Pycnogenol® on the climacteric syndrome in peri-menopausal women.* Acta Obstetricia et Gynecologica Scandinavica, 2007. **86**(8): p. 978–985.

35. Liu, X., et al., *Pycnogenol®, French maritime pine bark extract, improves endothelial function of hypertensive patients.* Life Sciences, 2004. **74**(7): p. 855–862.

36. Grether-Beck, S., et al., *French maritime pine bark extract (Pycnogenol®) effects on human skin: Clinical and molecular evidence.* Skin Pharmacology and Physiology, 2016. **29**(1): p. 13–17.

37. Cisár, P., et al., *Effect of pine bark extract (Pycnogenol®) on symptoms of knee osteoarthritis.* Phytotherapy Research, 2008. **22**(8): p. 1087–1092.

38. Bayer, J., et al., *Impact of a dietary supplementation with French maritime pine bark extract Pycnogenol® on salivary and serum inflammatory biomarkers during non-surgical periodontal therapy—A randomized placebo-controlled double-blind trial.* Nutrients, 2025. **17**(9): p. 1546.

39. Alan, L., et al., *Mitochondrial metabolism and hypoxic signaling in differentiated human cardiomyocyte AC16 cell line.* Am J Physiol Cell Physiol, 2025. **328**(5): p. C1571–c1585.

40. Okatan, E.N., et al., *Azoramide improves mitochondrial dysfunction in palmitate-induced insulin resistant H9c2 cells.* Mol Cell Biochem, 2019. **461**(1–2): p. 65–72.

41. Hosseinpourshirazi, F., et al., *Liraglutide Modulates Zinc Release and Improves Mitochondrial Function in Insulin-Resistant Senescent Cardiomyocytes.* Cardiovascular Toxicology, 2026. **26**(2): p. 22.

42. Li, Y., et al., *UBE3A alleviates isoproterenol-induced cardiac hypertrophy through the inhibition of the TLR4/MMP-9 signaling pathway.* Acta Biochimica et Biophysica Sinica, 2020. **52**(1): p. 58–63.

43. He, K., et al., *Chlorogenic acid attenuates isoproterenol Hydrochloride-induced cardiac hypertrophy in AC16 cells by inhibiting the Wnt/β-Catenin signaling pathway.* Molecules, 2024. **29**(4): p. 760.

44. Olgar, Y., A. Durak, and B. Turan, *Acute GLP-1 Agonism Induces Arrhythmogenic Electrical Activity in Aged Mice Heart Through Impaired Cellular Na + and Ca2 + Handlings: The Role of CK2 Hyperphosphorylation.* Anatol J Cardiol, 2025. **29**(2): p. 83–94.

45. Ramshesh, V.K. and J.J. Lemasters, *Imaging of mitochondrial pH using SNARF-1.* Methods Mol Biol, 2012. **810**: p. 243–8.

46. van Erp, P.E., et al., *Ratiometric measurement of intracellular pH in cultured human keratinocytes using carboxy-SNARF-1 and flow cytometry.* Cytometry, 1991. **12**(2): p. 127–32.

47. Olgar, Y., et al., *Aging related functional and structural changes in the heart and aorta: MitoTEMPO improves aged-cardiovascular performance.* Experimental Gerontology, 2018. **110**: p. 172–181.

48. Song, M., et al., *Mitochondrial Fission and Fusion Factors Reciprocally Orchestrate Mitophagic Culling in Mouse Hearts and Cultured Fibroblasts.* Cell Metabolism, 2015. **21**(2): p. 273–286.

49. Ong, S.-B., et al., *Inhibiting Mitochondrial Fission Protects the Heart Against Ischemia/Reperfusion Injury.* Circulation, 2010. **121**(18): p. 2012–2022.

50. Safaeian, L., et al., *Cardioprotective effects of Pinus eldarica bark extract on adrenaline-induced myocardial infarction in rats.* Asian Pacific Journal of Tropical Biomedicine, 2023. **13**(4).

51. Hajhashemi, V., B. Zolfaghari, and P. Amin, *Anti-nociceptive and anti-inflammatory effects of hydroalcoholic extract and essential oil of Pinus eldarica in animal models.* Avicenna J Phytomed, 2021. **11**(5): p. 494–504.

52. Safaeian, L., et al., *Antioxidant and Anti-hyperlipidemic Effects of Bark Extract of Pinus eldarica in Dexamethasone-induced Dyslipidemic Rats.* Journal of Advances in Medical and Biomedical Research, 2019. **27**: p. 49–56.

53. Cui, Y.-Y., M. Daglia, and H. Ullah, *Editorial: Pine bark extract: nutrition and metabolism.* Frontiers in Nutrition, 2024. **Volume 11–2024**.

54. Kim, H.J., et al., *Microbial production of levulinic acid from glucose by engineered Pseudomonas putida KT2440.* Journal of Biotechnology, 2024. **395**: p. 161–169.

55. Shariati, H., et al., *Evaluation of Diuretic and Antioxidant Properties in Aqueous Bark and Fruit Extracts of Pine.* Curr Drug Discov Technol, 2021. **18**(1): p. 58–64.

56. Kim, T.Y., et al., *Control of Reactive Oxygen Species for the Prevention of Parkinson's Disease: The Possible Application of Flavonoids.* Antioxidants, 2020. **9**(7): p. 583.

57. Dogan, E., et al., *The Effect of Pycnogenol on Wound Healing in Diabetic Rats.* Ostomy Wound Management, 2017. **63**: p. 41–47.

58. Drieling, R.L., et al., *No Beneficial Effects of Pine Bark Extract on Cardiovascular Disease Risk Factors.* Archives of Internal Medicine, 2010. **170**(17): p. 1541–1547.

59. Jia, G., M.A. Hill, and J.R. Sowers, *Diabetic Cardiomyopathy.* Circulation Research, 2018. **122**(4): p. 624–638.

60. Dinkova-Kostova, A.T. and A.Y. Abramov, *The emerging role of Nrf2 in mitochondrial function.* Free Radical Biology and Medicine, 2015. **88**: p. 179–188.

61. Bai, W., et al., *A population-based phenome-wide association study of cardiac and aortic structure and function.* Nature Medicine, 2020. **26**(10): p. 1654–1662.

62. Kubli, D.A. and Å.B. Gustafsson, *Mitochondria and Mitophagy.* Circulation Research, 2012. **111**(9): p. 1208–1221.

63. Gomes, L.C., G.D. Benedetto, and L. Scorrano, *During autophagy mitochondria elongate, are spared from degradation and sustain cell viability.* Nature Cell Biology, 2011. **13**(5): p. 589–598.

Figures

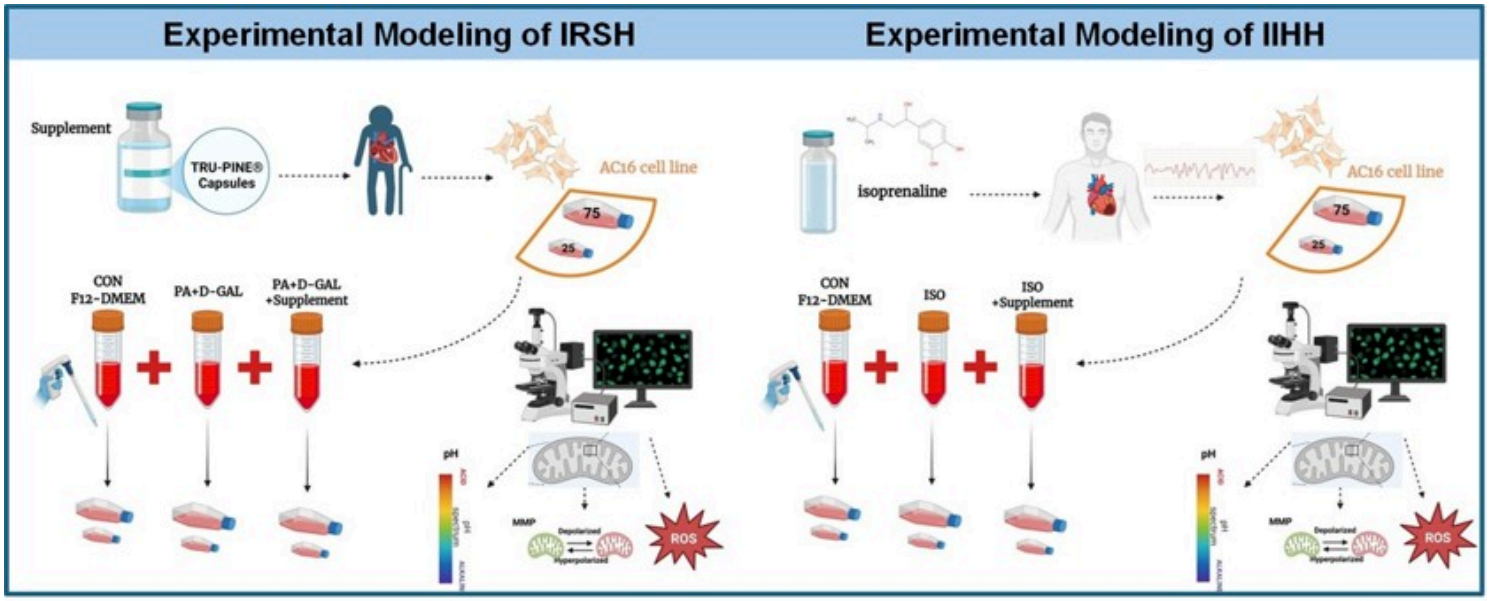


Figure 1

Figure 1

Experimental protocol for generating insulin-resistant senescent cardiomyocyte (IRSH) and isoproterenol (ISO)-induced hypertrophic cardiomyocyte (IIHH) models in AC16 human cardiomyocytes. AC16 cardiomyocytes were cultured and initially divided into three groups: control cells (Con), insulin-resistant senescent cells (IRSH; left), and ISO-induced hypertrophic cells (IIHH; right). Each experimental group was subsequently divided into untreated and CPBE-treated subgroups. Cells in the treatment subgroup received Canadian pine bark extract (CPBE), whereas the untreated subgroup was maintained under identical conditions without CPBE. Mitochondrial function, reactive oxygen species (ROS) production, and apoptosis-related parameters were assessed at the indicated time points (see Materials and Methods for details). All experiments were performed independently three times.

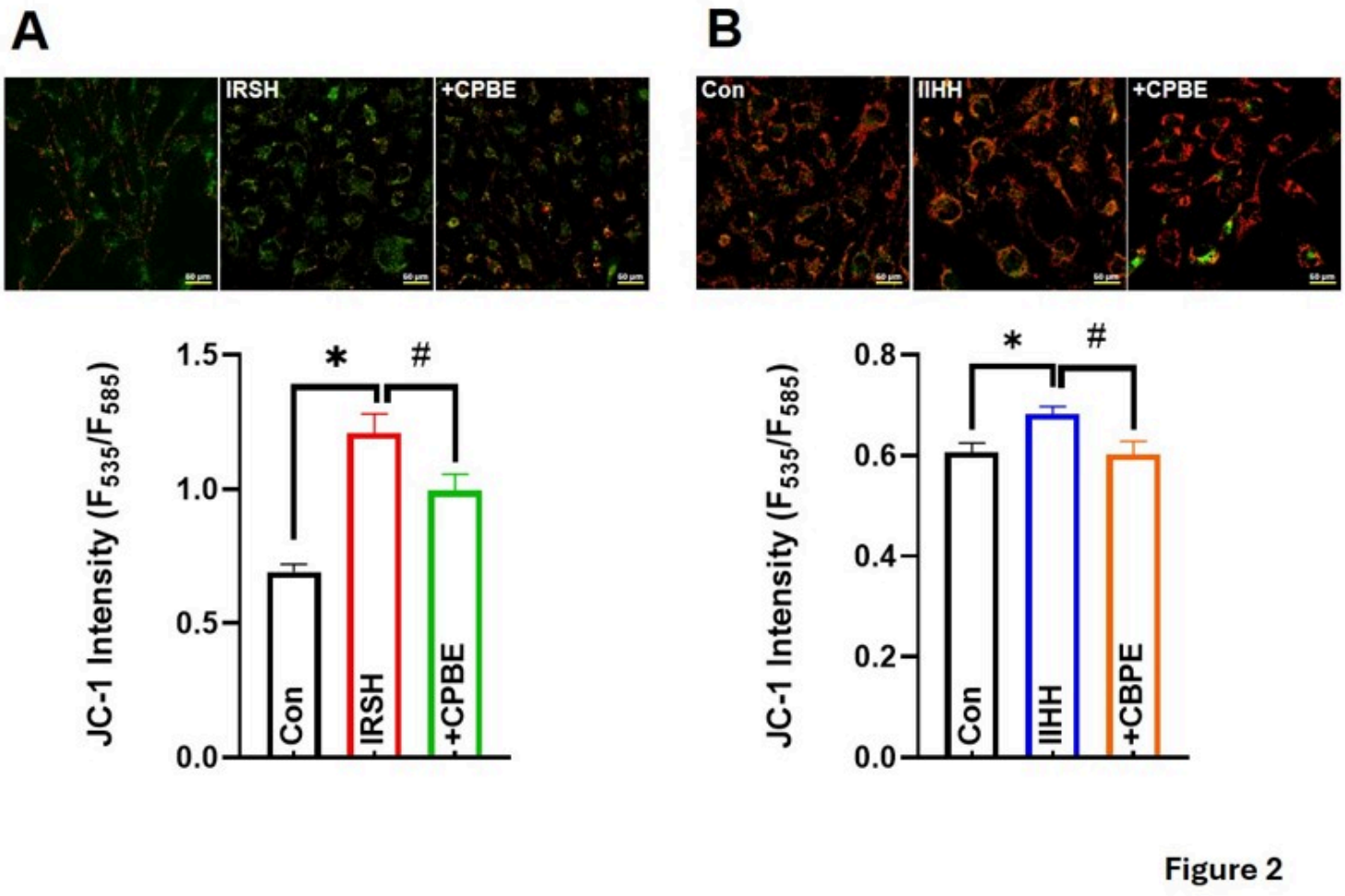


Figure 2

Figure 2

Assessment of mitochondrial membrane potential (MMP) in JC-1-stained AC16 cells using confocal microscopy. Representative ratiometric fluorescence images are shown above the corresponding bar graphs. MMP was evaluated in cells loaded with the membrane-permeable fluorescent probe JC-1 (5 μM, 30 min). JC-1 was excited at 488 nm, and fluorescence emissions were collected at 535 nm (green fluorescence, cytosolic monomers) and 585 nm (red fluorescence, mitochondrial aggregates). The numbers of analyzed cells were: Con = 40, IRSH = 20, IRSH+CPBE = 20, IIHH = 20, and IIHH+CPBE = 20 from three independent experiments. Data are presented as the mean ± SEM. Statistical analysis was performed using one-way ANOVA followed by Tukey's multiple comparisons test. *P*< 0.05 was considered statistically significant. *P* < 0.05 vs. Con; #*P* < 0.05 vs. IRSH or IIHH. Scale bar = 50 μm.

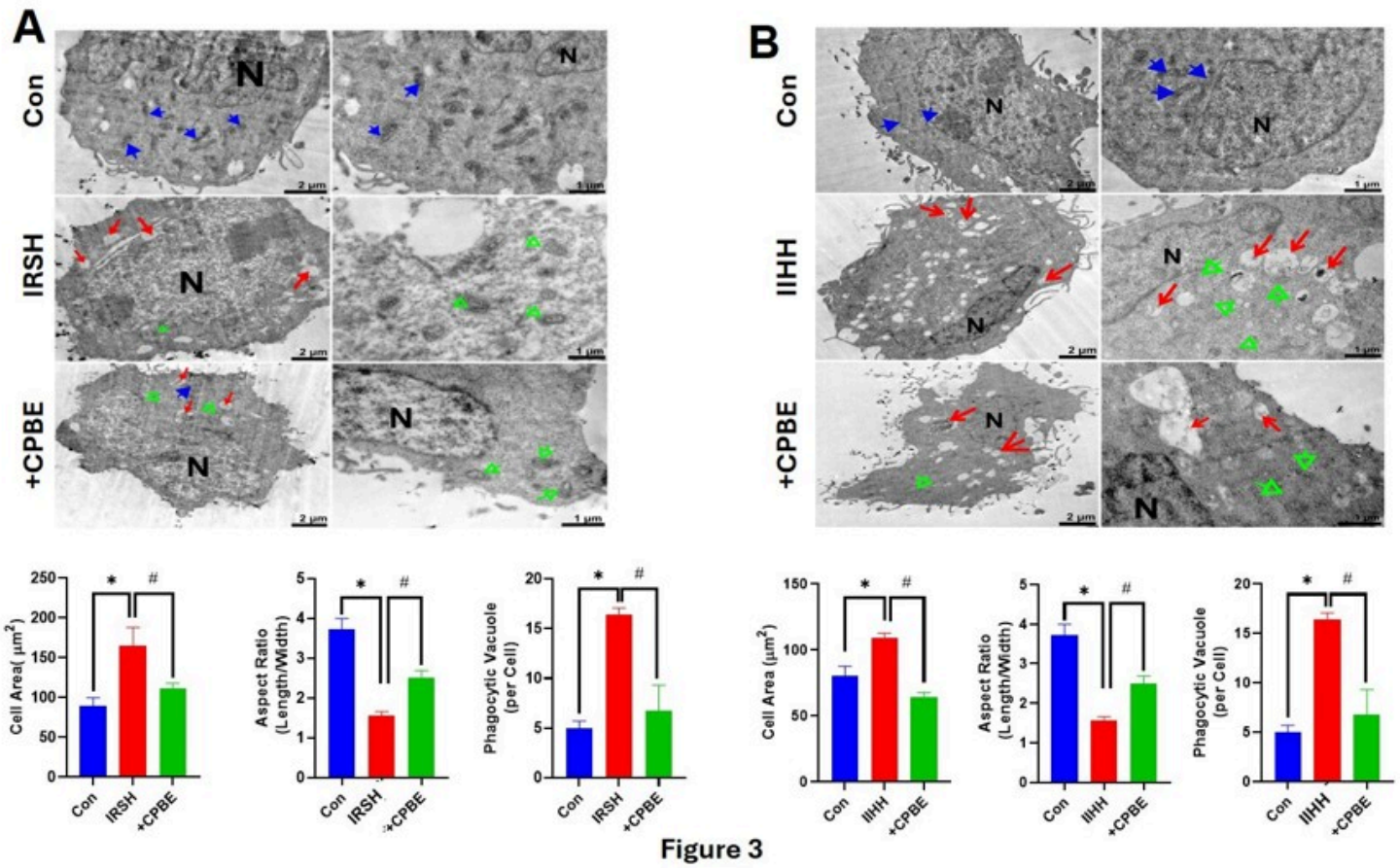


Figure 3

Figure 3

Transmission electron microscopy (TEM) analysis of mitochondrial ultrastructure in AC16 cells. TEM analyses were performed in Con, IRSH, and IRSH+CPBE cells (A, upper part) and in Con, IIHH, and IIHH+CPBE cells (B, upper part). Representative TEM micrographs illustrate mitochondrial ultrastructure in each experimental group. N, nucleus; blue arrows, normal mitochondria; green arrows, degenerative mitochondria exhibiting swelling and cristae disruption; red arrows, autophagic vacuoles containing mitochondrial remnants. (A) Con: ×6,000 and ×10,000. Mitochondria exhibited normal ultrastructural characteristics, including an elliptical morphology, well-organized cristae, and an electron-lucent matrix. IRSH: ×5,000 and ×10,000. Mitochondria appeared smaller with elliptical or rounded morphology and showed marked cristae disruption and loss. Numerous autophagic vacuoles were observed within the cytoplasm. IRSH+CPBE: ×5,000 and ×12,000. Although a small number of damaged mitochondria remained, many mitochondria displayed preserved ultrastructural morphology. The number of autophagic vacuoles was markedly reduced compared with the IRSH group. (B) Con: ×5,000 and ×10,000. Mitochondria displayed normal morphology with intact cristae and preserved matrix organization. IIHH: ×5,000 and ×10,000. Mitochondria were predominantly smaller and elliptical, exhibiting severe cristae disruption and structural disorganization. Autophagic vacuoles containing partially degraded mitochondrial material were frequently observed. IIHH+CPBE: ×5,000 and ×12,000. CPBE treatment reduced the number of autophagic vacuoles and partially restored mitochondrial ultrastructure. The quantitative analysis of mitochondrial ultrastructural alterations in TEM imaging

represented as cell area (down part, left), aspect ratio (lower part, middle) and phagocytic vacuole per cell (down part, right).

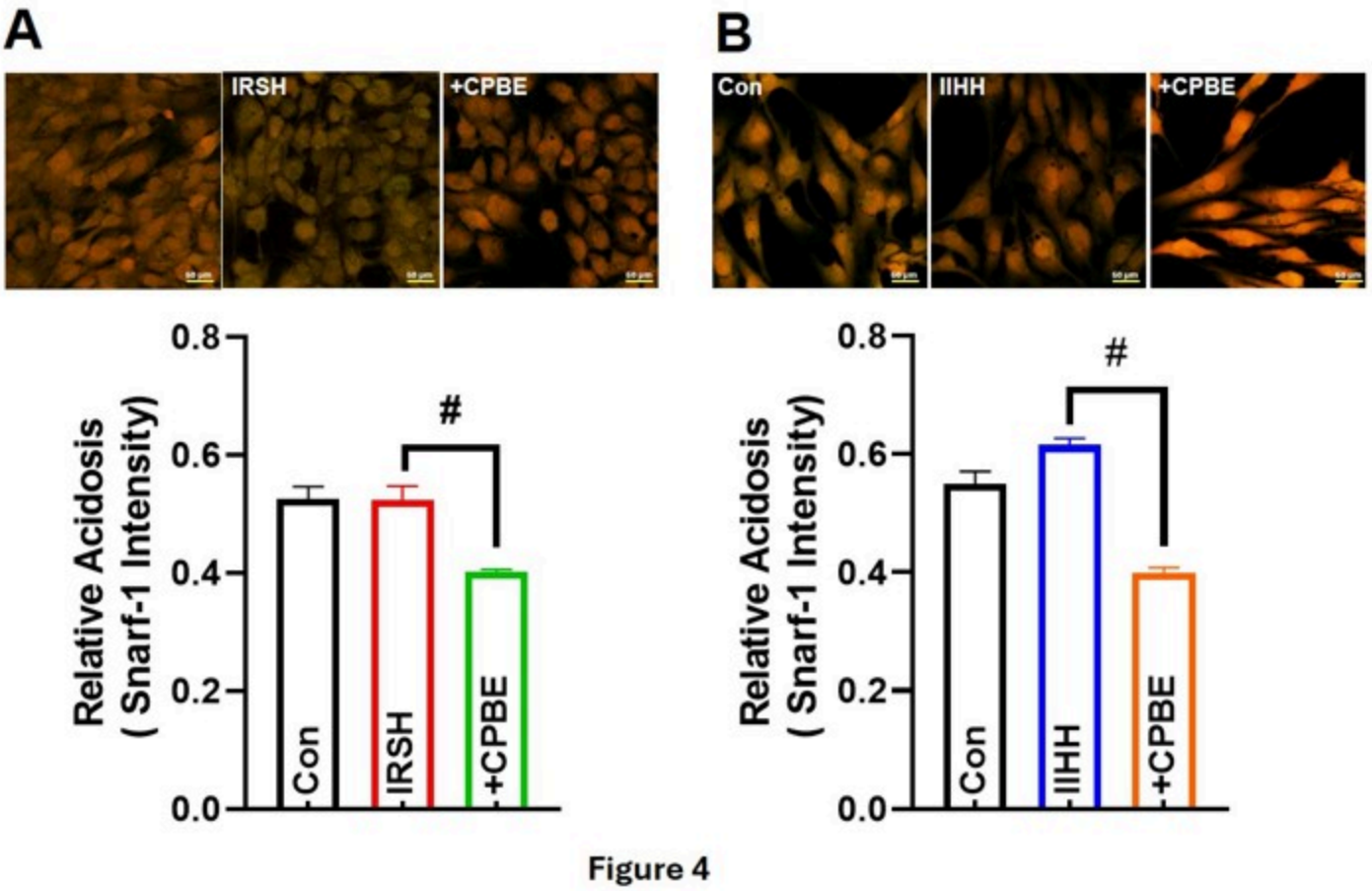


Figure 4

Figure 4

Assessment of intracellular pH in Snarf-1-stained AC16 cells using confocal microscopy. Representative ratiometric fluorescence images are shown above the corresponding bar graphs. Cells were loaded with the membrane-permeable fluorescent probe Snarf-1 AM (5 μM, 30 min at 37°C), and fluorescence imaging was performed using confocal microscopy. Excitation was performed at 543 nm, and emission signals were collected at 580 and 640 nm *(or 650 nm if appropriate—please use the correct wavelength consistently)*. Cytosolic pH was determined from the fluorescence intensity ratio (580/640 or 580/650 nm). Quantitative fluorescence data are presented for IRSH (A) and IIHH (B) cells relative to the Con group. The numbers of analyzed cells were: Con = 27, IRSH = 10, IRSH+CPBE = 10, IIHH = 15, and IIHH+CPBE = 19 from three independent experiments. Data are presented as the mean ± SEM. Statistical analysis was performed using one-way ANOVA followed by Tukey's multiple comparisons test. $P < 0.05$ was considered statistically significant. $P < 0.05$ vs. Con; #$P < 0.05$ vs. IRSH or IIHH. Scale bar = 50 μm.

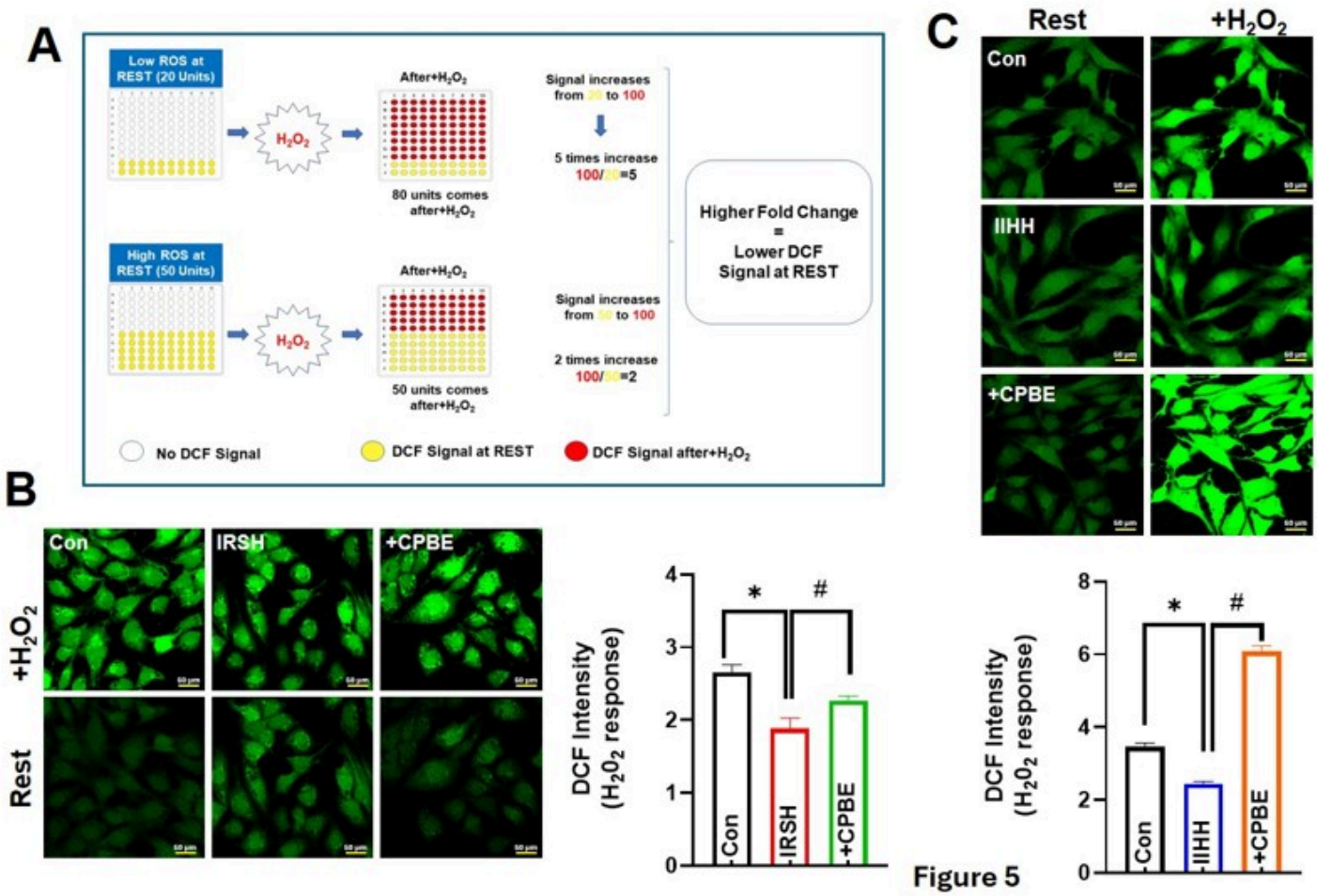


Figure 5

Assessment of intracellular reactive oxygen species (ROS) in DCFDA-stained AC16 cells using confocal microscopy. (A) Experimental protocol used for ROS measurements. Cells were loaded with the membrane-permeable ROS-sensitive fluorescent probe chloromethyl-2',7'-dichlorodihydrofluorescein diacetate (DCFDA, 10 μM) for 1 h. Following baseline fluorescence measurements, maximal ROS-dependent fluorescence was obtained by perfusion with HEPES-buffered solution containing H_2O_2 (100 μM). Representative fluorescence recordings are shown to the left of the corresponding bar graphs. Quantitative data obtained from IRSH (B) and IIHH (C) groups are presented as the mean ± SEM. The numbers of analyzed cells were: Con = 26, IRSH = 16, IRSH+CPBE = 15, IIHH = 15, and IIHH+CPBE = 15 from three independent experiments. Statistical analysis was performed using one-way ANOVA followed by Tukey's multiple comparisons test. *P*< 0.05 was considered statistically significant. *P* < 0.05 vs. Con; #*P* < 0.05 vs. IRSH or IIHH. Scale bar = 50 μm.

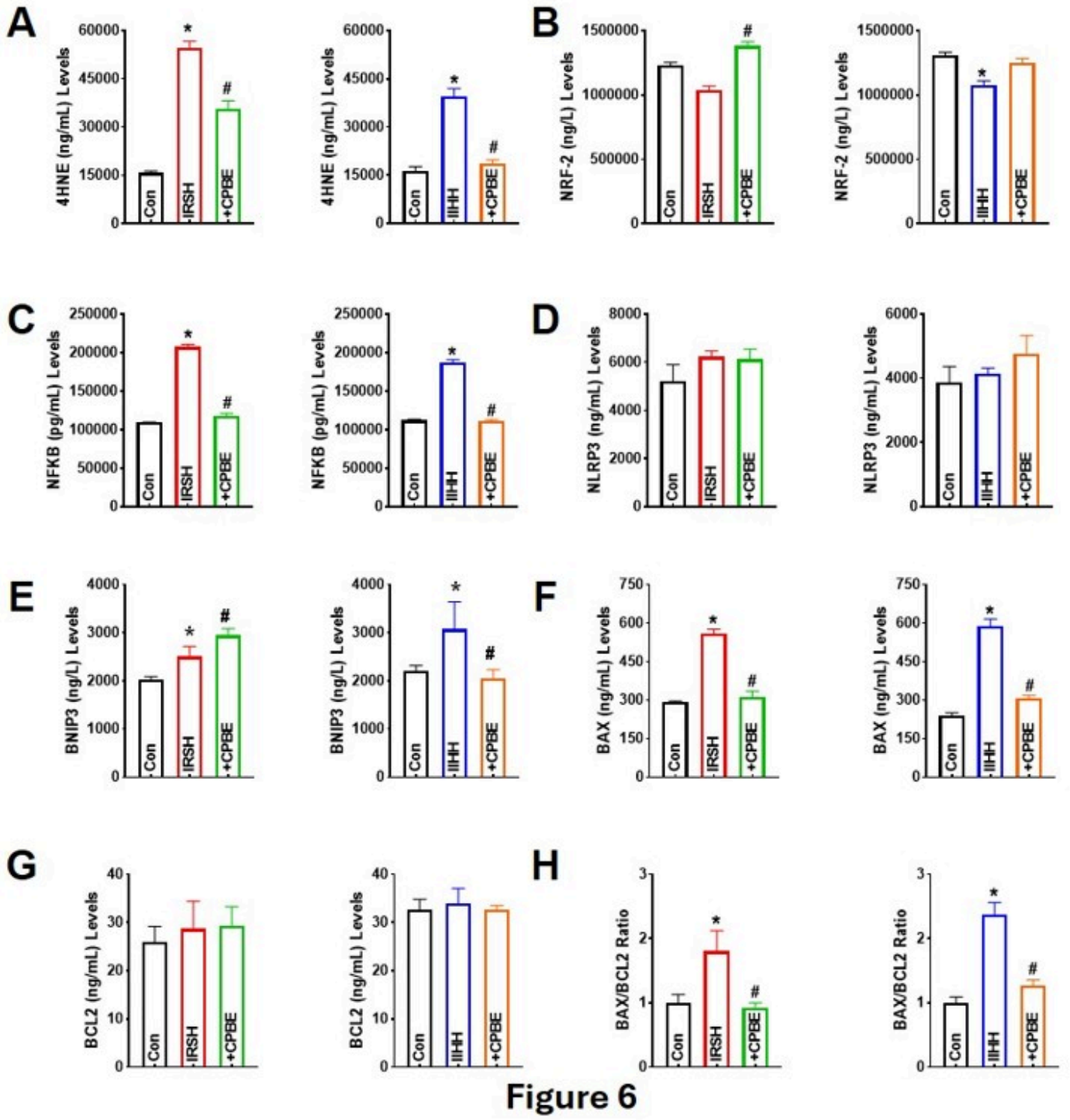


Figure 6

Effects of CPBE treatment on oxidative stress, inflammatory signaling, and apoptosis-related biomarkers in IRSH and IIHH cells. Oxidative stress was evaluated by measuring 4-HNE (A) and NRF2 (B). Inflammatory signaling was assessed by determining NF-κB (C) and NLRP3 (D) expression. Mitophagy-associated mitochondrial quality control was evaluated by measuring BNIP3 (E). Apoptosis was assessed by determining BCL-2 (F) and BAX (G) protein levels, and the BAX/BCL-2 ratio is presented in (H). Data for IRSH (left) and IIHH (right) groups are shown as the mean ± SEM from four independent

experiments. Statistical analysis was performed using the Kruskal–Wallis test followed by Bonferroni-adjusted multiple comparisons. $P < 0.05$ was considered statistically significant. $P < 0.05$ vs. Con; #$P < 0.05$ vs. IRSH or IIHH.

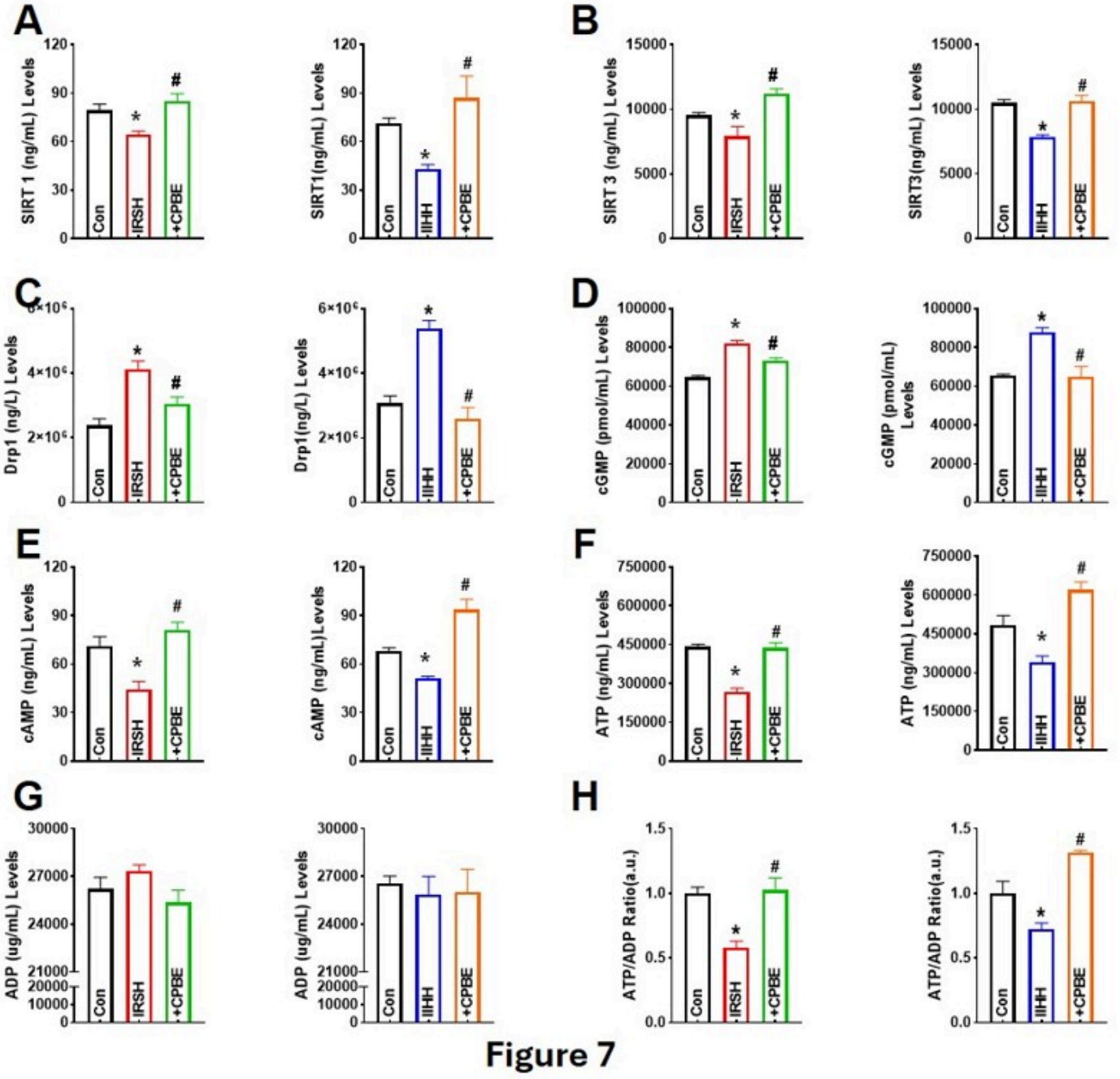


Figure 7

Figure 7

Effects of CPBE treatment on mitochondrial function-related parameters in IRSH and IIHH cells. The protein levels of the NAD^+-dependent deacetylases SIRT1 (A) and SIRT3 (B) are shown for both experimental groups relative to controls. DRP1, a key regulator of mitochondrial fission, is presented in (C). Cellular cGMP and cAMP levels are shown in (D) and (E), respectively. ATP and ADP levels are presented in (F) and (G), and the ATP/ADP ratio is shown in (H). Data from IRSH (left) and IIHH (right)

groups are presented as the mean ± SEM from four independent experiments. Statistical analysis was performed using the Kruskal–Wallis test followed by Bonferroni-adjusted multiple comparisons. $P < 0.05$ was considered statistically significant. $P < 0.05$ vs. Con; #$P < 0.05$ vs. IRSH or IIHH.

Supplementary Files

This is a list of supplementary files associated with this preprint. Click to download.

- floatimage6.jpeg